International Journal of Fluid Mechanics Research, 44(6):513–531 (2017)

NONLINEAR RADIATION EFFECT ON CASSON NANOFLUID PAST A PLATE IMMERSED IN DARCY–BRINKMAN POROUS MEDIUM WITH BINARY CHEMICAL REACTION AND ACTIVATION ENERGY

A. Zaib,[1,] M.M. Rashidi,[2] A.J. Chamkha,[3] & A.F. Al-Mudhaf[4]*

[1]*Department of Mathematical Sciences, Federal Urdu University of Arts, Science and Technology, Gulshan-e-Iqbal Karachi-75300, Pakistan*

[2]*Shanghai Automotive Wind Tunnel Center, Tongji University, 4800 Caoan Rd., Jiading, Shanghai 201804, China*

[3]*Mechanical Engineering Department, Prince Mohammad Bin Fahd University, Al-Khobar 31952, Saudi Arabia*

[4]*Manufacturing Engineering Department, The Public Authority for Applied Education and Training, Shuweikh 70654, Kuwait*

*Address all correspondence to: A. Zaib, Department of Mathematical Sciences, Federal Urdu University of Arts, Science and Technology, Gulshan-e-Iqbal Karachi-75300, Pakistan, E-mail: zaib20042002@yahoo.com

Original Manuscript Submitted: 1/19/2017; Final Draft Received: 4/17/2017

Nonlinear thermal radiation near a stagnation point of Casson nanofluid over a plate in a Darcy–Brinkman porous medium is considered. Combined effects of binary chemical reaction with activation energy are taken into account. For activation energy and thermal radiation a modified Arrhenius function and different type of Rosseland approximation are used. Similarity transformation is invoked to transform the governing equations including momentum, energy, and concentration into a system of highly nonlinear ordinary differential equations and solved numerically using a shooting method. Graphical results are shown in order to scrutinize the behavior of pertinent parameters on velocity, temperature, and concentration of nanoparticle. Also, the behavior of fluid flow is investigated through the coefficient of skin friction, the Nusselt number, the Sherwood number, and streamlines. It is observed that the thickness of the concentration boundary layer increases due to activation energy and decreases due to reaction rate and temperature differences. Finally, a comparative analysis is made through previous studies in limiting case.

KEY WORDS: *binary chemical reaction, activation energy, Casson nanofluid, porous medium, nonlinear thermal radiation*

1. INTRODUCTION

The process of mass transfer with binary chemical reaction and Arrhenius activation energy has been given a great deal of attention due to its various applications in chemical engineering such as cooling of nuclear reacting, geothermal reservoirs, and recovery of thermal oil. Generally, the relations between chemical reactions and mass transport are very complex, and can be scrutinized in the utilization of reactant species and production at several rates within the mass transfer and fluid. Bestman (1990) was the first who considered the combined effects of binary chemical reaction and Arrhenius activation energy on free convection flow with mass transfer in a vertical pipe immersed in a porous medium. He obtained the analytic solution using the perturbation method. Maleque (2013a) studied

NOMENCLATURE

c	positive constant
C_f	skin friction coefficient
C	concentration of nanoparticle
C_w	concentration of nanoparticle at the surface
C_∞	ambient concentration of nanoparticle
D_B	coefficient of Brownian diffusion [m^2s^{-1}]
D_T	coefficient of thermophoresis diffusion [m^2s^{-1}]
E_a	activation energy
E	dimensionless activation energy
e_{ij}	(i, j)th component of the deformation rate
f	dimensionless stream function
k	thermal conductivity [Wm^{-1} K]
k_r^2	chemical reaction rate constant
k^*	mean absorption coefficient
K	porous parameter
K_1	permeability of the porous medium [m^2]
m_w	mass flux
n	fitted rate constant
Nb	Brownian motion parameter
Nt	thermophoresis parameter
Nu_x	local Nusselt number
Pe_x	Péclet number
Pr	Prandtl number
P_y	yield stress of the fluid
q_r	radiative heat flux [kg m^{-1} s^{-3} K^{-1}]
q_w	heat flux [Wm^{-2}]
Re_x	local Reynolds number
N_d	thermal radiation parameter
Sc	Schmidt number
Sh_x	Sherwood number
T	temperature [K]
T_∞	free stream temperature [K]
T_w	fluid wall temperature [K]
u_e	free stream velocity [ms^{-1}]
u, v	velocity components [ms^{-1}]
x, y	Cartesian coordinates [m]

Greek Symbols

α	thermal diffusivity [m^2 s^{-1}]
β	dimensionless reaction rate
δ	temperature difference parameter
ε	porosity parameter of the porous medium
γ	Casson fluid parameter
κ	Boltzmann constant
φ	dimensionless concentration of nanoparticle
θ	dimensionless temperature
θ_w	temperature ratio parameter
ν	kinematic viscosity [m^2s^{-1}]
ν_{eff}	effective kinematic viscosity [m^2s^{-1}]
ρ	density [kgm^{-3}]
$(\rho c_p)_f$	specific heat capacitance of nanofluid [$Jm^{-3}K^{-1}$]
$(\rho c_p)_p$	effective heat capacitance of nanofluid [$Jm^{-3}K^{-1}$]
μ_B	viscosity of Casson fluid [N sm^{-2}]
μ_{eff}	effective (or "apparent") viscosity [N sm^{-2}]
τ	ratio of heat capacitance [JK^{-1}]
τ_w	shear stress in $x$direction [Nm^{-2}]
σ^*	Stefan–Boltzmann constant [kg s^{-3} K^{-4}]
ψ	stream function
η	similarity variable
Λ	modified porosity parameter

Subscripts

w	condition at wall
∞	condition at free stream

Superscripts

$'$	derivative w.r.t. η

magnetohydrodynamic (MHD) free convection flow and heat with mass transfer over a porous vertical plate with binary chemical reaction and Arrhenius activation energy in the presence of heat generation/absorption and viscous dissipation. In another paper, Maleque (2013b) studied the MHD unsteady free convection flow over a permeable flat plate with exothermic/endothermic chemical reactions, Arrhenius activation energy, and thermal radiation. The boundary layer flow and heat transfer using a two-equation energy model inside a channel embedded in porous medium was investigated by Rassoulinejad-Mousavi et al. (2013). The unsteady flow with heat and mass transfer past a stretching sheet with binary chemical reaction with Arrhenius activation energy in a rotating fluid was scrutinized by Awad et al. (2014). Recently, Shafique et al. (2016) studied the steady flow of a non-Newtonian Maxwell fluid past an elastic surface in a rotating frame in the presence of binary chemical reaction along with activation energy.

Casson fluid is known as a non-Newtonian fluid because of its rheological behavior in relation to shear stress–strain relationship. At lower shear strain Casson fluid acts like a solid and acts like Newtonian fluid above the value of critical stress. A few Casson fluids examples are tomato sauce, jelly, human blood, honey, and many more. Also, when blood moves through small vessels at low shear rates, this flow is explained by the model of Casson fluid (McDonald, 1974; Shaw et al., 2009). Therefore, it is significant to undertake the study of Casson fluid. Mustafa et al. (2012) examined the steady flow of a Casson fluid with heat transfer near a stagnation point toward a stretching sheet. The mixed convective flow of a Casson fluid near a stagnation point toward a stretching surface was studied by Hayat et al. (2012). Shehzad et al. (2013) investigated MHD flow with mass transfer of a Casson fluid past a permeable stretching sheet. Bhattacharyya et al. (2014) obtained an exact solution of Casson fluid flow over a permeable shrinking sheet. Isa et al. (2014) obtained the multiple solutions of a mixed convective Casson fluid flow near a stagnation point over a permeable vertical plate. Abolbashari et al. (2015) scrutinized the effect of entropy generation with heat and mass transfer of a Casson nanofluid over a heated stretching sheet with partial slip. Prasad et al. (2016a) investigated MHD flow and heat transfer of a Casson nanofluid past a stretching sheet with fluid variable properties. The influences of Brownian diffusion and thermophoresis on non-Newtonian Casson fluid containing nanoparticles past a nonlinear stretching surface was investigated by Prasad et al. (2016b). Zaib et al. (2016) obtained the dual solutions of Casson fluid flow and heat transfer toward an exponentially shrinking sheet in the presence of viscous dissipation. Recently, Prasad et al. (2017) discussed the impact of variable fluid properties on electrically conducting fluid with heat and mass transfer over a vertical stretching sheet.

In recent years, nanotechnology has grabbed the distinct attention of various authors because of its massive applications in modern technology. It has also been observed in recent years that enhancement of heat transfer in mechanical and thermal systems is encountered. Nanofluid is a fluid that is formed by scattering nanometer-sized solid particles and/or fibers having diameter less than 100 nm. Since regular heat-transfer fluids (for instance water, bio-fluids, engine oil, and ethylene glycol) have lower thermal conductivities which cannot congregate with the requirement of modern technologies of cooling, Choi and Eastman (1995) dispersed the particles made of metal or metal oxide into regular fluids to enhance the thermal conductivity. Since the thermal conductivity of nanofluids is much higher than the regular or convectional fluids, Buongiorno (2006) observed that the Brownian motion parameter and thermophoresis diffusion effect of nanoparticles give the massive enhancement in the thermal conductivity of fluid. Due to these effects, he suggested the modifications in the convective situations. Nield and Kuznetsov (2009, 2010) initially examined the boundary layer flow of a nanofluid along a vertical surface. Later on, Khan and Pop (2010) extended the work of Nield and Kuznetsov by considering a constant surface temperature over a stretching surface. Rana and Bhargava (2012) investigated the steady flow of a nanofluid past a nonlinear stretching surface. Rashidi et al. (2013) studied electrically conducting flow of a nanofluid using the second law of thermodynamics past a porous rotating disk. The heat generation effect on free convective flow of a nanofluid past a vertical plate immersed in a non-Darcy porous medium was studied by Chamkha et al. (2014). Beg et al. (2014) obtained the numerical solution of single-phase and two-phase models in a circular tube filled with Al_2O_3–water-based nanofluid. Rashidi et al. (2014) compared numerically the single-phase and two-phase with heat transfer characteristic and flow field in a wavy channel filled with copper–water nanofluid. Garoosi et al. (2015) investigated free and mixed convection flow of three types of nanofluid, namely Cu, Al_2O_3, and TiO_2, in a cavity. Freidoonimehr et al. (2015) studied MHD unsteady free convection flow of a four different water-based nanofluid toward a porous vertical stretching surface. Liu et al. (2016) developed an approach containing optomechanical actuator nanoparticle to control the tension receptor optically in living cells. The reliability of the dual embedded atom method based on copper, aluminum, and nickel interatomic potentials for predicting the elastic properties was investigated by Rassoulinejad-Mousavi et al. (2016). Rahman et al. (2016) investigated the effects of Brownian motion and thermophoresis diffusion using the second law of thermodynamics of a non-Newtonian Jeffrey nanofluid past a stretching surface with zero flux. Recently, Vajravelu et al. (2017) examined the characteristics of fluid variable property on electrically conducting squeezing nanofluid between parallel disk in the presence of transpiration.

Generally, porous medium is significant for storage of energy and transport. The study of flow in a porous medium has played an important role in many engineering and scientific applications. This nature of flow is essential in a large range of technical problems, for example design of packed bed reactor, oil recovery techniques, environmental pollution, thermal insulation, centrifugal separation of particles, heat storage system, and blood rheology.

More applications can be seen in the books by Bejan et al. (2004); Vafai (2005), and Vadasz (2008). The Darcy law expresses as the proportionality between the pressure gradient and the velocity that has been employed to study the variety of fluids problem in saturated porous medium. This model, however, is only valid for slow flows with low permeability through porous media, whereas certain porous materials such as foam metals and fibrous media usually have high porosities (Harris et al., 2009). In porous media, inertia effects and boundary are not considered in Darcy's model which may change the flow characteristics with heat and mass transfer. Thus, it is very important to determine under what conditions these effects are significant. The most comprehensive and accurate model for transport through porous media is the Darcy–Brinkman–Forchheimer equation. While the nonlinear drag term (Forchheimer number) disabled researchers from presenting analytical solution at large values of Forchheimer number for finding the behavior of fluid flow and heat transfer at those real situations, Rassoulinejad-Mousavi and Abbasbandy (2011) solved the challenge and succeeded to present an analytical model to investigate this behavior at any value of influential parameters. They showed that in some values of Darcy number ($Da = K/R^2$, which is related to K here) the effect of Forchheimer number may not be significant and may be neglected for ease of computations. This investigation for different channels and physics has been considered in Rassoulinejad-Mousavi and Abbasbandy, 2011; Rassoulinejad-Mousavi et al., 2014; Rassoulinejad-Mousavi and Yaghoobi, 2014 as well. Based on Rassoulinejad-Mousavi and Abbasbandy, 2011; Rassoulinejad-Mousavi et al., 2014; Rassoulinejad-Mousavi and Yaghoobi, 2014, for the sake of simplicity and convergence of results one neglects the nonlinear drag term and uses the linear Darcy–Brinkman model. Hong et al. (1987) have revealed that for the no-slip condition the Brinkman (1947) model should be used, which is the extension of Darcy's law. Later on, Ishak et al. (2008) used this model to investigate the steady flow near the stagnation point over a vertical sheet immersed in a porous medium with wall temperature. Rosali et al. (2011) investigated the mixed convective flow near the stagnation point toward a vertical plate immersed in a porous medium in the presence of variable heat flux. The boundary layer flow inside a permeable channel for Darcy–Brinkman equations with suction/injection was scrutinized by Seyf and Rassoulinejad-Mousavi (2011). Shirazpour et al. (2011) obtained the analytic solution of fully developed flow in a channel embedded in a Darcy–Brinkman porous medium with Lorentz force. The mix convection flow with heat transfer over a heated vertical surface immersed in a Darcy–Brinkman porous medium was examined by Pantokratoras (2014). Recently, Pantokratoras (2015) studied forced convective flow with heat transfer past a plane sheet in the presence of convective boundary condition in a Darcy–Brinkman porous medium.

In view of such facts the prime interest of the current communication is to examine the effects of binary chemical reaction with activation energy and nonlinear thermal radiation on stagnation point by dispersing nanoparticles in non-Newtonian Casson fluid past a plate in a Darcy–Brinkman porous medium. The transformed nonlinear differential equations are solved numerically using the shooting method. The impacts of all physical parameters of interest are discussed numerically and graphically. To the best of the authors' knowledge no one has yet considered this type of problem.

2. PROBLEM FORMULATION

Consider a steady two-dimensional incompressible fluid toward the stagnation-point of Casson nanofluid over a plate immersed in a Darcy–Brinkman porous medium as shown in Fig. 1. The x axis is taken along the plate and the y axis perpendicular to it. Binary chemical reaction with activation energy and nonlinear thermal radiation are invoked. It is considered that external velocity $u_e(x) = cx$ varies linearly from the stagnation point, where c is positive constant. Further, wall temperature T_w and wall concentration C_w as well as ambient temperature T_∞ and ambient concentration C_∞ are considered as constant. The Brownian motion and thermophoresis effects are presented. We shall use the Brinkman–Darcy model, where the velocity square term is neglected. For an isotropic flow the rheological equation of state of Casson fluid is expressed as

$$\Gamma_{ij} = \begin{cases} \left(\mu_B + \dfrac{p_y}{\sqrt{2\pi}}\right) 2e_{ij}, & \pi > \pi_c, \\ \left(\mu_B + \dfrac{p_y}{\sqrt{2\pi_c}}\right) 2e_{ij}, & \pi < \pi_c, \end{cases} \tag{1}$$

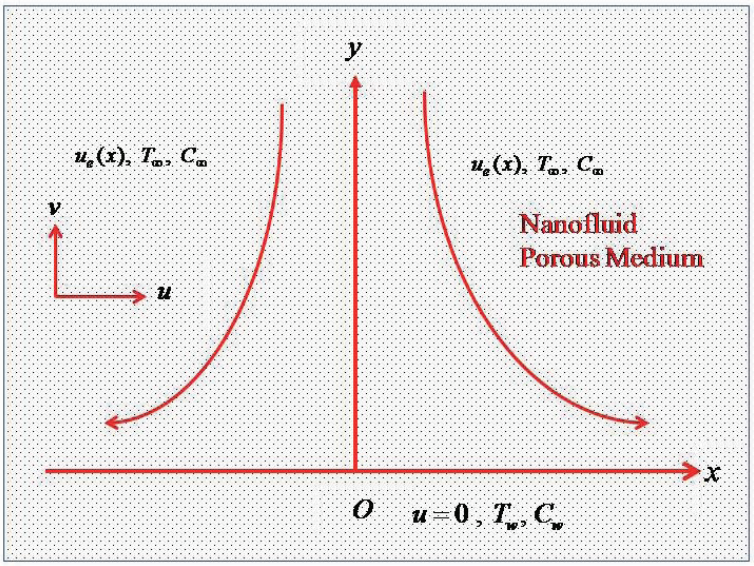

FIG. 1: Physical diagram of the problem

where e_{ij} is the strain tensor rate, μ_B is the viscosity of Casson fluid, p_y is the yield stress of fluid, $\pi = e_{ij}e_{ji}$ is the product of the component of deformation rate with itself, and π_c is the critical value of the product of the component of the strain tensor rate with itself. The governing equations under these assumptions with the usual boundary layer are written as

$$\frac{\partial u}{\partial x} + \frac{\partial v}{\partial y} = 0, \tag{2}$$

$$u\frac{\partial u}{\partial x} + v\frac{\partial u}{\partial y} - u_e\frac{du_e}{dx} = \varepsilon^2\nu_{eff}\left(1+\frac{1}{\gamma}\right)\frac{\partial^2 u}{\partial y^2} - \frac{\varepsilon^2\nu}{K_1}(u-u_e), \tag{3}$$

$$u\frac{\partial T}{\partial x} + v\frac{\partial T}{\partial y} = \alpha\frac{\partial^2 T}{\partial y^2} + \tau\left[D_B\frac{\partial C}{\partial y}\frac{\partial T}{\partial y} + \left(\frac{D_T}{T_\infty}\right)\left(\frac{\partial T}{\partial y}\right)^2\right] - \frac{1}{(\rho c_p)_f}\frac{\partial q_r}{\partial y}, \tag{4}$$

$$u\frac{\partial C}{\partial x} + v\frac{\partial C}{\partial y} = D_B\frac{\partial^2 C}{\partial y^2} + \left(\frac{D_T}{T_\infty}\right)\left(\frac{\partial T^2}{\partial y^2}\right) - k_r^2\left(\frac{T}{T_\infty}\right)^n e^{-(E_a/\kappa T)}(C - C_\infty). \tag{5}$$

The physical boundary conditions are

$$\begin{aligned} &u = 0,\ v = 0,\ T = T_w,\ C = C_w \text{ at } y = 0,\\ &u \to u_e(x),\ T \to T_\infty,\ C \to C_\infty \text{ as } y \to \infty, \end{aligned} \tag{6}$$

where u and v are the velocity components in the x and y directions, respectively, $\nu_{eff} = \mu_{eff}/\rho$ is the effective kinematic viscosity, μ_{eff} is the effective (or "apparent") viscosity, ρ is the density, ν is the normal kinematic viscosity, ε is the porosity parameter of the porous medium, K_1 is the permeability of the porous medium, α is the thermal diffusivity, k is the fluid thermal conductivity, T is the temperature, T_∞ is the ambient temperature, C is the concentration of nanoparticle, D_B and D_T are the coefficients of Brownian and thermophoresis diffusion, respectively, τ is the ratio between the effective heat capacity of the nanoparticle material and specific heat capacitance of the fluid, $(\rho c_p)_f$ is the specific heat capacitance of nanofluid, $k_r^2(T/T_\infty)^n e^{-(E_a/\kappa T)}$ and κ are the modified Arrhenius function and the Boltzmann constant, respectively, where k_r^2 is the chemical reaction rate constant and n is the fitted rate constant, which lies between $-1 < n < 1$.

Following Khan et al. (2016), the radiative heat flux q_r is expressed as

$$q_r = -\frac{4\sigma^*}{3k^*}\frac{\partial T^4}{\partial y} = -\frac{16\sigma^*}{3k^*}T^3\frac{\partial T}{\partial y}, \tag{7}$$

where σ^* is the Stefan–Boltzmann constant and k^* is the mean absorption coefficient. Using Eq. (7), energy equation (4) can be written as

$$u\frac{\partial T}{\partial x} + v\frac{\partial T}{\partial y} = \frac{\partial}{\partial y}\left[\left(\alpha + \frac{16\sigma^* T^3}{3(\rho c_p)_f k^*}\right)\frac{\partial T}{\partial y}\right] + \tau\left[D_B\frac{\partial C}{\partial y}\frac{\partial T}{\partial y} + \left(\frac{D_T}{T_\infty}\right)\left(\frac{\partial T}{\partial y}\right)^2\right]. \tag{8}$$

Now, we introduce the similarity transformation (Rosali et al., 2011):

$$\eta = y\sqrt{\frac{c}{\alpha}}, \quad \psi = \sqrt{c\alpha}xf(\eta), \quad \theta(\eta) = \frac{T - T_\infty}{T_w - T_\infty}, \quad \varphi(\eta) = \frac{C - C_\infty}{C_w - C_\infty}. \tag{9}$$

Here η is the similarity variable, ψ is the stream function, and we get $T = T_\infty\left[1 + (\theta_w - 1)\,\theta\right]$ with $\theta_w > 1$, where $\theta_w = T_w/T_\infty$ is the temperature ratio parameter.

In view of relation (9), Eqs. (3)–(8) are transformed into the following ordinary differential equations:

$$\Lambda\left(1 + \frac{1}{\gamma}\right)f''' + ff'' - f'^2 + K\,(1 - f') + 1 = 0, \tag{10}$$

$$\theta'' + f\theta' + \frac{4}{3N_d}\frac{d}{d\eta}\left[\{1 + (\theta_w - 1)\,\theta\}^3\,\theta'\right] + Nb\theta'\varphi' + Nt\,(\theta')^2 = 0, \tag{11}$$

$$\varphi'' + \mathrm{Sc}\,f\varphi' + \frac{Nt}{Nb}\theta'' - \beta\mathrm{Sc}\,(1 + \delta\theta)^n\exp\left(-\frac{E}{1 + \delta\theta}\right)\varphi = 0, \tag{12}$$

subject to the boundary conditions

$$\begin{aligned} &f(0) = 0, \quad f'(0) = 0, \quad \theta(0) = 1, \quad \phi(0) = 1, \\ &f'(\infty) \to 1, \quad \theta(\infty) \to 0, \quad \phi(\infty) \to 0, \end{aligned} \tag{13}$$

where primes denote differentiation with respect to η, $\Lambda = \varepsilon^2\mathrm{Pr} = \varepsilon^2\nu_{eff}/\alpha$ is the modified permeability parameter, $K = \varepsilon^2\nu/cK_1$ is the porosity parameter, $\gamma = \mu_B\sqrt{2\pi_c}/p_y$ is the Casson parameter, $Nb = \tau D_B\,(C_w - C_\infty)/\nu$ is the Brownian motion parameter, $Nt = \tau D_T\,(T_w - T_\infty)/T_\infty\nu$ is the thermophoresis parameter, $N_d = kk^*/4\sigma^* T_\infty^3$ is the thermal radiation parameter, $E = E_a/\kappa T_\infty$ is the dimensionless activation energy, $\beta = k_r^2/c$ is the nondimensional reaction rate, $\delta = (T_w - T_\infty)/T_\infty$ is the temperature difference parameter, and $\mathrm{Sc} = \nu/D_B$ is the Schmidt number.

The important physical quantities of interest are the skin friction coefficient, the Nusselt number, and the Sherwood number, which are written as

$$C_{fx} = \frac{\tau_w}{\rho u_w^2}, \quad \mathrm{Nu}_x = -\frac{xq_w}{k(T_w - T_w)}, \quad \mathrm{Sh}_x = \frac{xm_w}{D_B(C_w - C_\infty)}, \tag{14}$$

where τ_w is the shear stress, q_w is the heat flux, and m_w is the mass flux given as

$$\tau_w = \left(\mu_B + \frac{p_y}{\sqrt{2\pi}}\right)\left(\frac{\partial u}{\partial y}\right)_{y=0}, \quad q_w = -k\left(\frac{\partial T}{\partial y}\right)_w + (q_r)_w, \quad m_w = -D_B\left(\frac{\partial C}{\partial y}\right)_{y=0}. \tag{15}$$

Using Eq. (8), we get

$$\begin{aligned} C_f\mathrm{Re}_x^{1/2}/\mathrm{Pr}^{1/2} &= \left(1 + \frac{1}{\gamma}\right)f''(0), \quad \mathrm{Sh}_x\mathrm{Pe}_x^{-1/2} = -\phi'(0), \\ \mathrm{Nu}_x\mathrm{Pe}_x^{-1/2} &= -\left[1 + \frac{4}{3R_d}\{1 + (\theta_w - 1)\,\theta(0)\}^3\right]\theta'(0), \end{aligned} \tag{16}$$

where $\mathrm{Re}_x = xu_e/\nu$ is the Reynolds number and $\mathrm{Pe}_x = xu_e/\alpha$ is the Péclet number.

3. RESULTS AND DISCUSSION

The transformed nonlinear equations (10)–(12) with the boundary conditions (13) were numerically solved using the shooting method. The obtained numerical results for different physical parameters involving in the problem are discussed through graphs and tables. Table 1 displays the comparison of our results of $f''(0)$ with the results of Yacob et al. (2011) and Hamad et al. (2012), which shows good agreement.

Figures 2–4 elucidate the effect of Casson parameter γ on the velocity profile, temperature distribution, and concentration of nanoparticle. Figure 2 shows an increasing behavior in velocity profile with increasing values of γ. Thus the Casson parameter reduces the thickness of the velocity boundary layer. Physically, the yield stress reduces due to increasing values of γ, which causes the decline of velocity boundary layer thickness. The temperature distribution and concentration of nanoparticle decrease due to increasing values of γ as shown in Figs. 3 and 4, respectively. The

TABLE 1: Comparison of $f''(0)$ when $K = 0$, $\Lambda = 1$, $\gamma \to \infty$

Yacob et al. (2011)	Hamad et al. (2012)	Present
1.2326	1.232588	1.2326

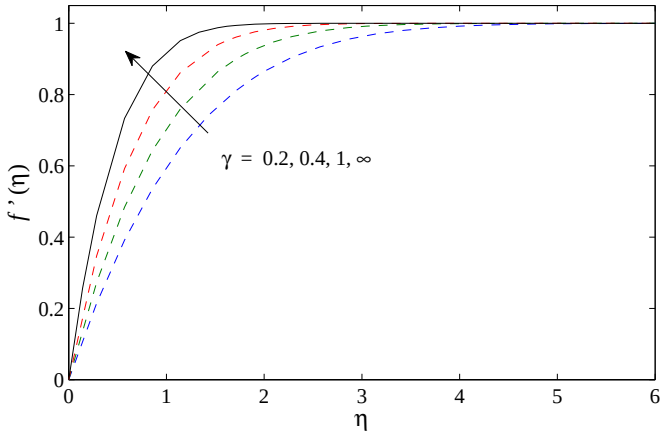

FIG. 2: Velocity profile for different values of γ when $\Lambda = 0.5$, $K = 0.5$

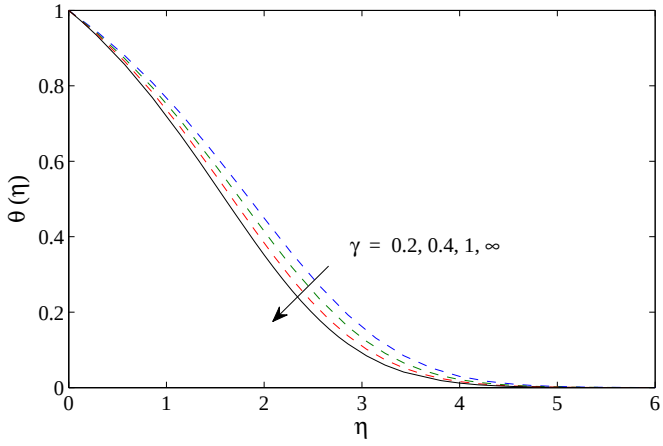

FIG. 3: Temperature profile for different values of γ when $\Lambda = 0.5$, $K = 0.5$, $Nb = 1.5$, $Nt = 0.5$, $Q_w = 1.5$, $N_d = 2$

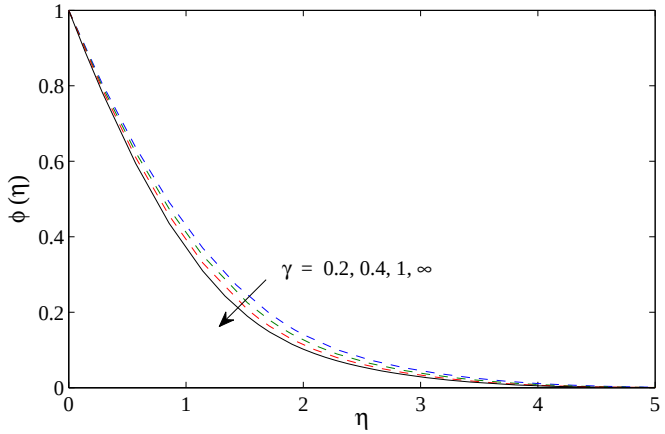

FIG. 4: Concentration of nanoparticle for different values of γ when $\Lambda = 0.5$, $K = 0.5$, $Nb = 1.5$, $Nt = 0.5$, $Q_w = 1.5$, $N_d = 2$, $\beta = 2$, $E = 3$, $n = \delta = 0.5$, Sc = 1

thinning of the thermal as well as the concentration boundary layer thicknesses happens due to the elasticity stress parameter. It is also seen from these figures that as we enhance the Casson parameter, i.e., $\gamma \to \infty$, the non-Newtonian behavior disappears and the fluid behaves like a Newtonian fluid. Further, the thicknesses of velocity, thermal, and concentration boundary layers are smaller for Casson fluid compared to Newtonian fluid.

Figures 5–7 demonstrate the velocity profile f', temperature distribution θ, and concentration of nanoparticle φ for different values of modified permeability parameter Λ. Figure 5 illustrates that the velocity profile shows a decreasing behavior with increasing values of Λ. Therefore, the thickness of the velocity boundary layer becomes thicker and thicker. In contrast, temperature profile and concentration nanoparticle increase as Λ increases and consequently increase the thermal as well as concentration boundary layer thicknesses as shown in Figs. 6 and 7, respectively.

Figures 8–10 elucidate the effect of porosity parameter K on the velocity profile, temperature distribution, and concentration of nanoparticle. Figure 8 reveals that the velocity of fluid increases with K and consequently decreases the velocity boundary layer thickness. Physically, as the porous parameter increases, the regime becomes more porous and as a result the Darcian force moderates in magnitude. This resistance of Darcian force behaves to decelerate the

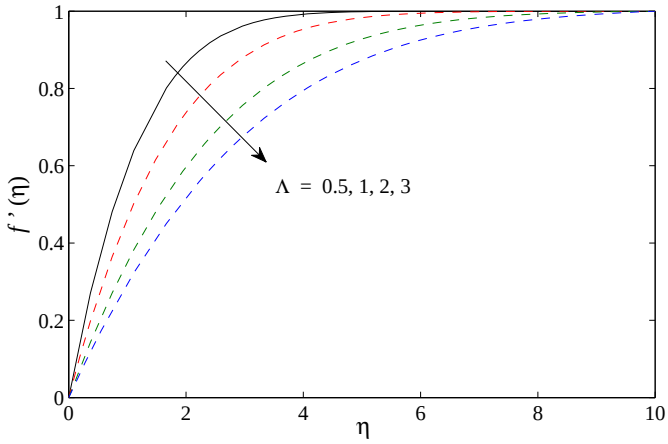

FIG. 5: Velocity profile for different values of Λ when $\gamma = 0.2$, $K = 0.5$

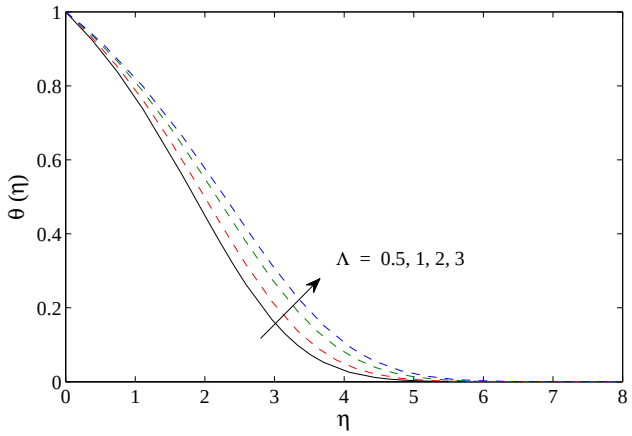

FIG. 6: Temperature profile for different values of Λ when γ = 0.2, K = 0.5, Nb = 1.5, Nt = 0.5, Q_w = 1.5, N_d = 2

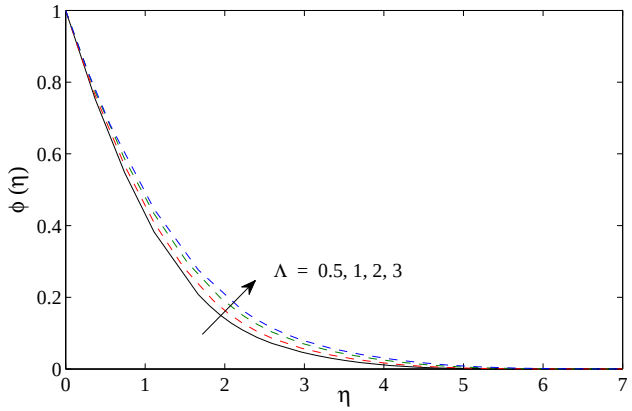

FIG. 7: Concentration of nanoparticle for different values of Λ when γ = 0.2, K = 0.5, Nb = 1.5, Nt = 0.5, Q_w = 1.5, N_d = 2, β = 2, E = 3, n = δ = 0.5, Sc = 1

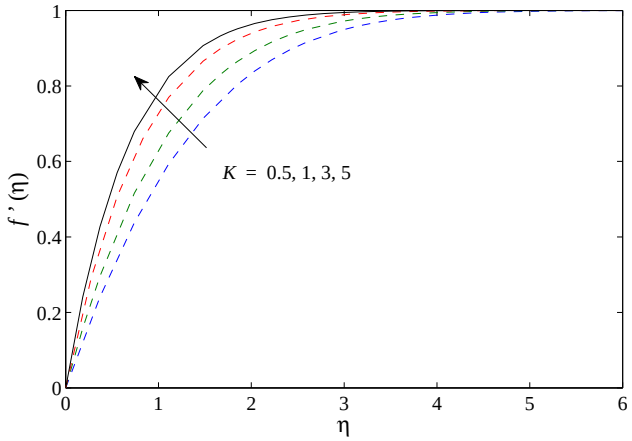

FIG. 8: Velocity profile for different values of K when γ = 0.2, Λ = 0.5

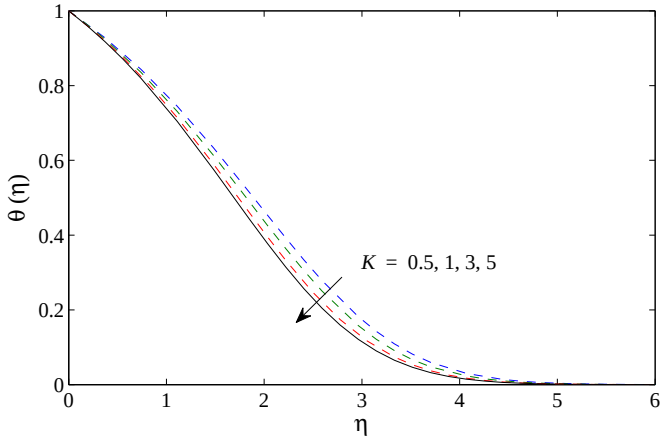

FIG. 9: Temperature profile for different values of K when $\gamma = 0.2$, $\Lambda = 0.5$, $Nb = 1.5$, $Nt = 0.5$, $Q_w = 1.5$, $N_d = 2$

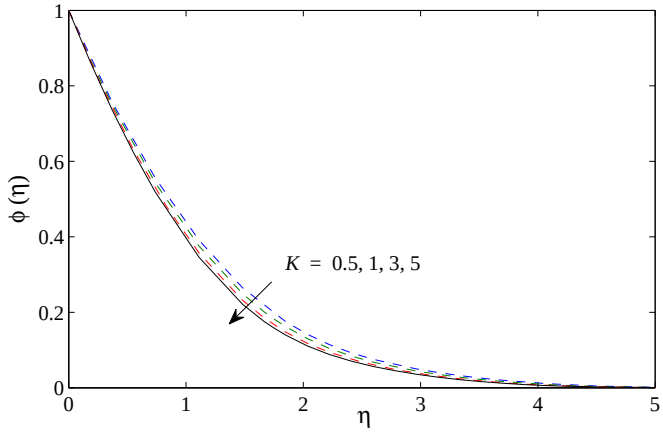

FIG. 10: Concentration of nanoparticle for different values of Λ when $\gamma = 0.2$, $K = 0.5$, $Nb = 1.5$, $Nt = 0.5$, $Q_w = 1.5$, $N_d = 2$, $\beta = 2$, $E = 3$, $n = \delta = 0.5$, Sc = 1

fluid's particles. This reduces the resistance as the porous parameter increases. So, gradually the flow experiences less drag and thereby decreases the flow retardation. Hence, the porous parameter boosts the fluid motion within the boundary layer, whereas the temperature distribution and concentration of nanoparticle decrease with increasing values of K, forcing the thermal and concentrations profiles to become thinner and thinner as shown in Figs. 9 and 10, respectively.

Figures 11 and 12 are prepared to show the Brownian motion effect Nb on the temperature distribution and concentration of nanoparticle, respectively. Figure 11 elucidates that the temperature distribution and thermal boundary layer thickness increase with increasing Nb. The physical reason is that the kinetic energy of the nanoparticles increases due to the strength of this chaotic motion and as a result, the fluid's temperature increases, whereas the opposite trend is seen on the concentration of nanoparticle as depicted in Fig. 12. It can be seen that the concentration of nanoparticle decreases due to increasing values of Nb. It can be concluded that the Brownian motion parameter makes the fluid warm within the boundary and at that time aggravates deposition particles away from the regime of fluid to the surface, causing a decrease in concentration of nanoparticle as well as the thickness of the boundary layer. The larger values of Brownian motion imply the strong behavior for the smaller particle, whereas for the stronger

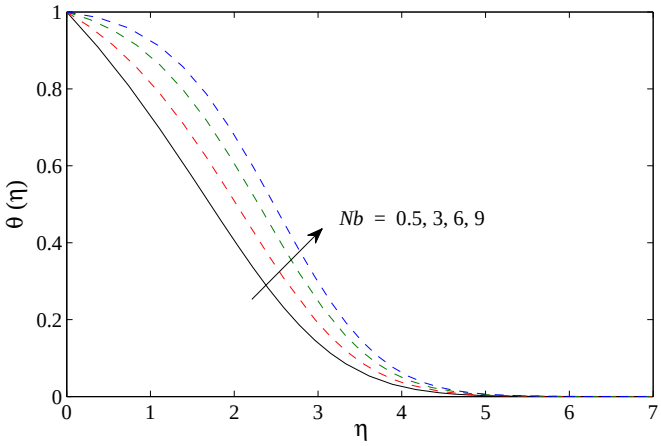

FIG. 11: Temperature profile for different values of Nb when $\gamma = 0.5$, $\Lambda = 0.5$, $K = 0.5$, $Nt = 0.5$, $Q_w = 1.5$, $N_d = 2$

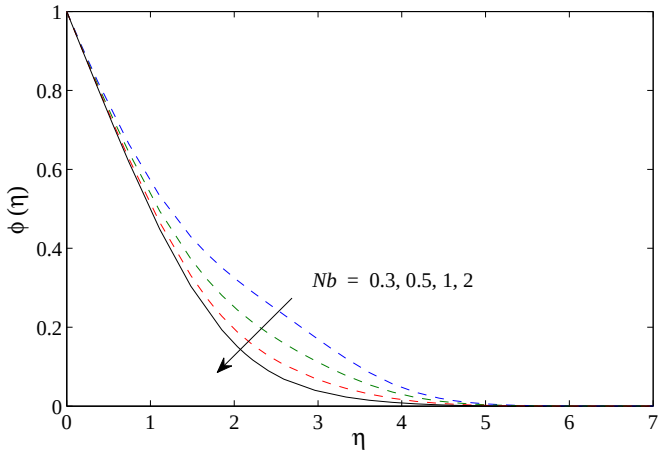

FIG. 12: Concentration of nanoparticle for different values of Nb when $\gamma = 0.5$, $\Lambda = 0.5$, $K = 0.5$, $Nt = 0.5$, $Q_w = 1.5$, $N_d = 2$, $\beta = 10$, $E = 10$, $n = \delta = 0.5$, Sc = 1

particle the smaller values of Nb are applied. The impact of thermophoresis parameter Nt on the temperature distribution and concentration nanoparticle is presented in Figs. 13 and 14, respectively. Figures 13 and 14 show that the temperature distribution and concentration nanoparticle increase with increasing Nt. This is because diffusion penetrates deeper into the fluid due to increasing values of Nt, which cause the thickening of the thermal boundary layer as well as the concentration boundary layer. The effect of the thermophoresis parameter is more pronounced on the concentration of nanoparticle compared to temperature distribution.

Figure 15 elucidates the increasing behavior in concentration nanoparticle due to increasing values of nondimensional activation energy E and leads to an increase of the concentration boundary layer thickness. Physically, higher activation energy and lower temperature lead to a lesser reaction rate, which slows down the chemical reaction. Figure 16 preserves the influence of temperature difference δ on the concentration profile. This result showed that the concentration nanoparticle and concentration boundary layer thickness decrease due to increasing values of δ. Figure 17 shows that due to increasing values of dimensionless reaction rate β, the concentration nanoparticle decreases and leads to thinning the concentration boundary layer thickness. Physically, an increase in the value of β leads to

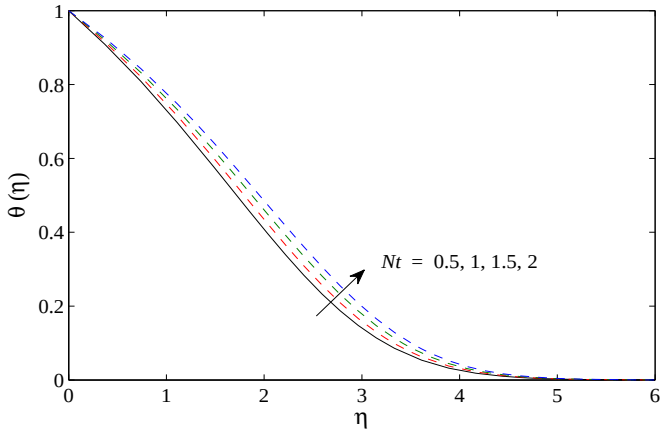

FIG. 13: Temperature profile for different values of Nt when $\gamma = 0.5$, $\Lambda = 0.5$, $K = 0.5$, $Nb = 0.5$, $Q_w = 1.5$, $N_d = 2$

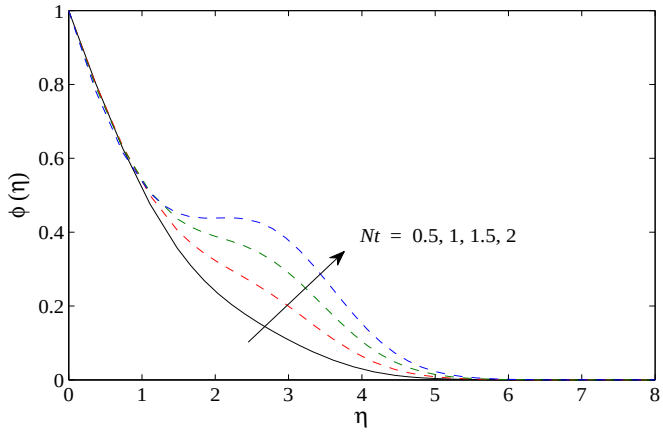

FIG. 14: Concentration of nanoparticle for different values of Nt when $\gamma = 0.5$, $\Lambda = 0.5$, $K = 0.5$, $Nb = 0.5$, $Q_w = 1.5$, $N_d = 2$, $\beta = 4$, $E = 5$, $n = \delta = 0.2$, Sc = 1

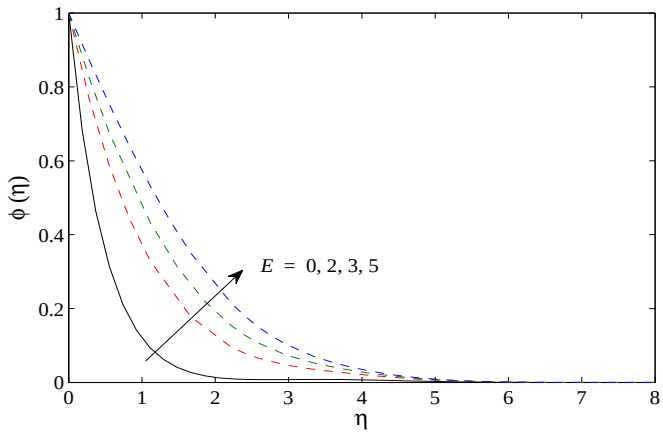

FIG. 15: Concentration of nanoparticle for different values of E when $\gamma = 0.2$, $\Lambda = 3$, $K = 0.5$, $Nb = 1.5$, $Nt = 0.5$, $Q_w = 1.5$, $N_d = 2$, $\beta = 4$, $n = \delta = 0.2$, Sc = 1

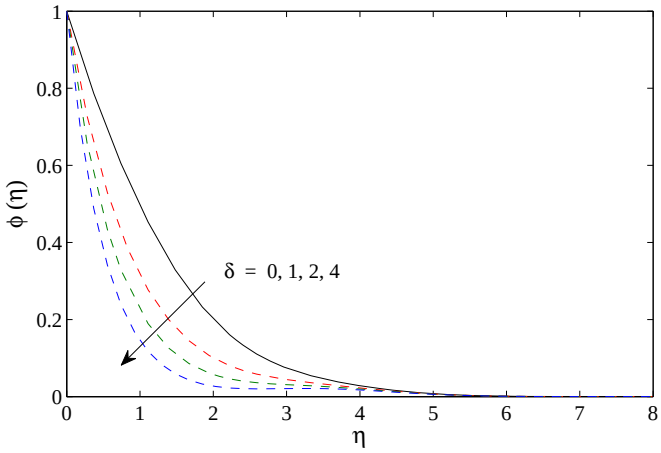

FIG. 16: Concentration of nanoparticle for different values of δ when γ = 0.2, Λ = 3, K = 0.5, Nb = 1.5, Nt = 0.5, Q_w = 1.5, N_d = 2, E = 3, β = 5, n = 0.2, Sc = 1

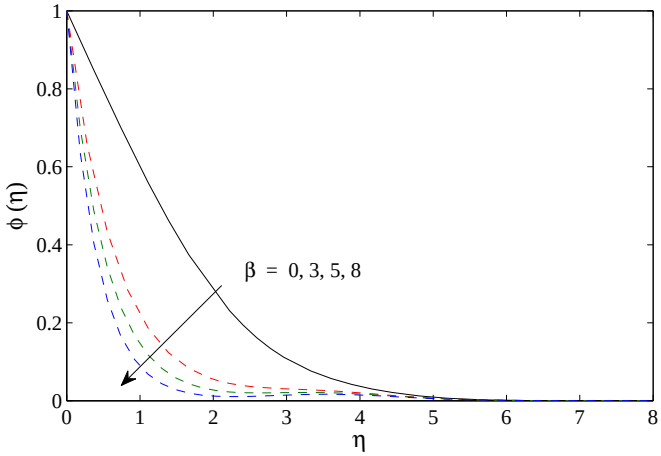

FIG. 17: Concentration of nanoparticle for different values of β when γ = 0.2, Λ = 3, K = 0.5, Nb = 1.5, Nt = 0.5, Q_w = 1.5, N_d = 2, δ = 3, E = 3, n = 0.2, Sc = 1

an increase in the term $\beta\,(1+\delta\theta)^n \exp\left(-E/1+\delta\theta\right)$. This ultimately helps the destructive chemical reaction that increases the concentration.

Figure 18 demonstrates the influence of radiation parameter N_d on the temperature distribution. This figure shows a decreasing behavior for increasing N_d. Thus, the thermal boundary layer thickness becomes thinner and thinner. This is because a large value of the radiation parameter implies the dominance of conduction and therefore, the thermal boundary layer thickness decreases.

Figures 19–21 scrutinize the effect of the Casson parameter γ versus Λ on the skin friction, the Nusselt number, and the Sherwood number. As expected, the value of the skin friction decreases due to increasing values of γ, whereas the Nusselt number and the Sherwood number increase with increasing γ. The values of skin friction, the Nusselt number, and the Sherwood number significantly drop as Λ increases. It is also observed from these figures that the values at the surface are higher for a porous medium $(K \neq 0)$ compared to clear fluid $(K = 0)$. Further, the values of the skin friction, the Nusselt number, and the Sherwood number are positive. Physically, positive values of the skin

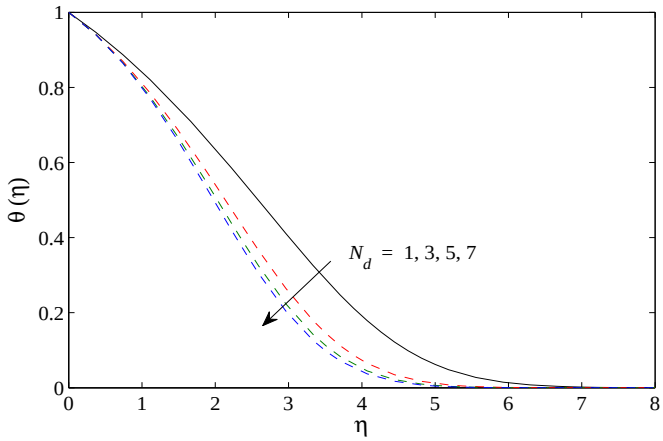

FIG. 18: Temperature profile for different values of N_d when $\gamma = 0.2$, $\Lambda = 3$, $K = 0.5$, $Nb = 1.5$, $Nt = 0.5$, $Q_w = 1.5$

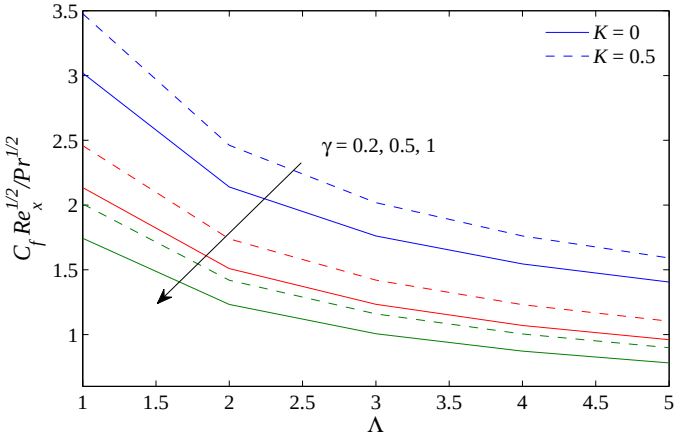

FIG. 19: Skin friction versus Λ for different values of γ

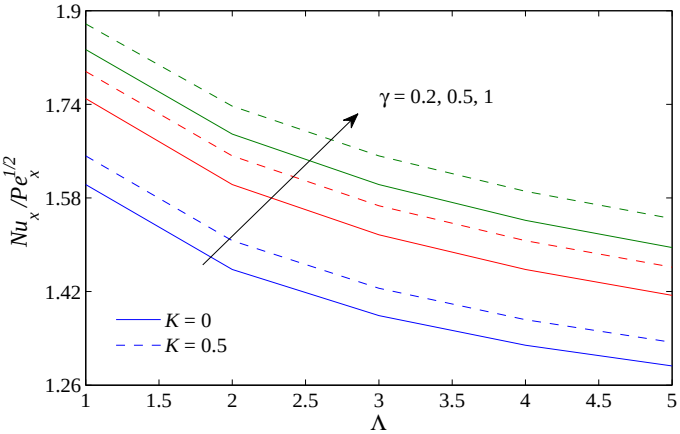

FIG. 20: Nusselt number versus Λ for different values of γ when $Nb = 1.5$, $Nt = 0.5$, $N_d = 2$, $Q_w = 1.5$

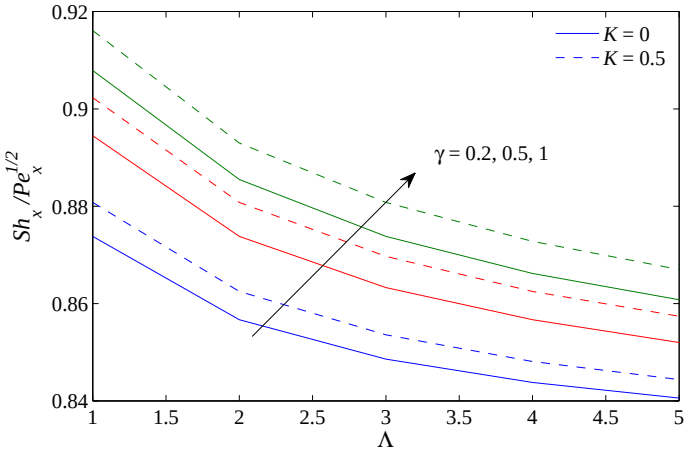

FIG. 21: Sherwood number versus K for different values of Λ when Nb = 1.5, Nt = 0.5, Q_w = 1.5, N_d = 2, β = 4, δ = 0.5, E = 3, n = 0.5, Sc = 1

friction imply that the fluid applies a drag force on the hard surface, while for positive values of the Nusselt number it means that heat is moved from the hot place to the cold fluid. This behavior is also tabulated in Table 2.

TABLE 2: Values of the skin friction, the Nusselt number, and the Sherwood number versus Λ for different values of γ when Nb = 1.5, Nt = 0.5, Sc = 1, Q_w = 1.5, N_d = 2, E = 3, β = 4, δ = 0.5, n = 0.5 are fixed

γ	K	Λ	$C_f\mathrm{Re}_x^{1/2}/\mathrm{Pr}^{1/2}$	$\mathrm{Nu}_x/\mathrm{Pe}_x^{1/2}$	$\mathrm{Sh}_x/\mathrm{Pe}_x^{1/2}$
0.2	0	1	3.0194	1.6029	0.8738
		2	2.1401	1.4578	0.8567
		3	1.7613	1.3789	0.8486
	0.5	1	3.4778	1.6519	0.8808
		2	2.4617	1.5069	0.8625
		3	2.0181	1.4257	0.8536
0.5	0	1	2.1349	1.7498	0.8945
		2	1.5097	1.6029	0.8738
		3	1.2334	1.5171	0.8633
	0.5	1	2.4591	1.7961	0.9023
		2	1.7389	1.6519	0.8808
		3	1.4201	1.5666	0.8697
1	0	1	1.7431	1.8336	0.9079
		2	1.2326	1.6891	0.8855
		3	1.0065	1.6029	0.8738
	0.5	1	2.0078	1.8774	0.9161
		2	1.4198	1.7368	0.8930
		3	1.1593	1.6519	0.8808

Finally, the sketched streamlines using stream function ψ are illustrated in Figs. 22 and 23 for Newtonian fluid $(\gamma \to \infty)$ and non-Newtonian Casson fluid, respectively. These figures signify that streamlines are moderately simple, symmetric, and fuller toward an axis but there is a slight difference in streamlines of non-Newtonian fluid compared to streamlines of Newtonian fluid.

4. CONCLUSIONS

This research analyzed the consequences of binary chemical reaction and activation energy on stagnation point flow of a Casson nanofluid past a plate in a Darcy–Brinkman porous medium. The shooting method is used to obtain the numerical solutions of converted nonlinear differential equations. The important findings of this research regarding the various pertinent parameters were gathered. The velocity of fluid increases due to the porosity parameter, whereas the velocity decreases due to the modified permeability parameter. The temperature of the fluid and concentration of the nanoparticle decrease due to the porosity parameter and increase as the modified parameter increases. The Casson parameter enhances the velocity of the fluid, whereas the temperature distribution and concentration nanoparticle

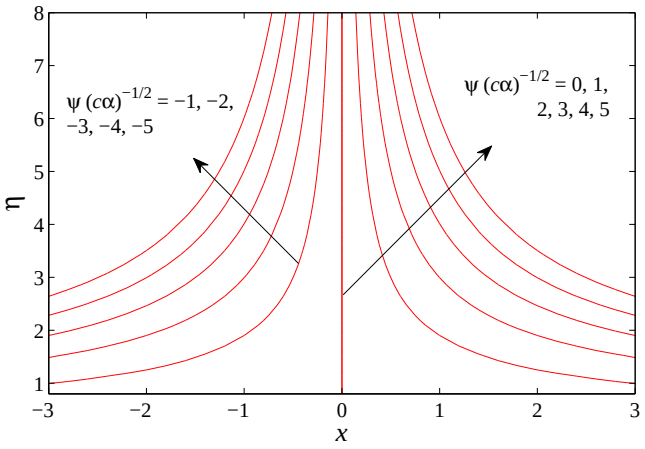

FIG. 22: Streamline pattern when $\Lambda = 0.5$, $\beta \to \infty$, $K = 0.5$

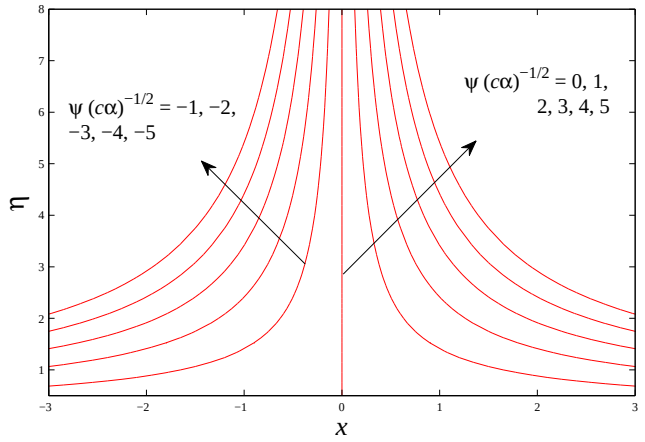

FIG. 23: Streamline pattern when $\Lambda = 0.5$, $\beta = 0.2$, $K = 0.5$

decrease. Further, the temperature distribution and concentration of nanoparticle increase as the thermophoresis parameter increases. Increasing values of the Brownian motion parameter lead to increase the temperature of fluid and decreases the concentration of nanoparticle. Moreover, the thermal radiation reduces the temperature of fluid, whereas the temperature difference parameter and dimensionless reaction parameter reduce the concentration of nanoparticle, while the profile enhances due to the activation energy parameter. The skin friction decreases with increasing values of γ, whereas the Nusselt number and the Sherwood number increase. Higher values are seen for porous medium compared to clear fluid.

REFERENCES

Abolbashari, M.H., Freidoonimehr, N., Nazari, F., and Rashidi, M.M., Analytical modeling of entropy generation for Casson nano-fluid flow induced by a stretching sheet, *Adv. Powder Technol.*, vol. **26**, pp. 542–552, 2015.

Awad, F.G., Motsa, S., and Khumalo, M., Heat and mass transfer in unsteady rotating fluid flow with binary chemical reaction and activation energy, *PLoS One*, vol. **9**, pp. 1–12, 2014.

Beg, O.A., Rashidi, M.M., Akbari, M., and Hosseini, A., Comparative numerical study of single-phase and two-phase models for bio-nanofluid transport phenomena, *J. Mech. Med. Biol.*, vol. **14**, pp. 1–31, 2014.

Bejan, A., Dincer, I., Lorente, S., Miguel, A.F., and Reis, A.H., *Porous and Complex Flow Structures in Modern Technologies*, New York: Springer, 2004.

Bestman, A.R., Natural convection boundary layer with suction and mass transfer in a porous medium, *Int. J. Eng. Res.*, vol. **14**, no. 4, pp. 389–396, 1990.

Bhattacharyya, K., Hayat, T., and Alsaedi, A., Exact solution for boundary layer flow of Casson fluid over a permeable stretching/shrinking sheet, *Z. Angew. Math. Mech.*, vol. **94**, pp. 522–528, 2014.

Brinkman, H.C., On the permeability of media consisting of closely packed porous particles, *Appl. Sci. Res.*, vol. **1**, pp. 81–86, 1947.

Buongiorno, J., Convective transport in nanofluids, *ASME J. Heat Transfer*, vol. **128**, pp. 240–250, 2006.

Chamkha, A.J., Rashad, A.M., Ram Reddy, Ch., and Murthy, P.V.S.N., Effect of suction/injection on free convection along a vertical plate in a nanofluid saturated non-Darcy porous medium with internal heat generation, *Indian J. Pure Appl. Math.*, vol. **45**, pp. 321–342, 2014.

Choi, S.U.S. and Eastman, J.A., Enhancing thermal conductivity of fluids with nanoparticles, *ASME FED*, vol. **231**, pp. 99–105, 1995.

Freidoonimehr, N., Rashidi, M.M., and Mahmud, S., Unsteady MHD free convective flow past a permeable stretching vertical surface in a nano-fluid, *Int. J. Thermal Sci.*, vol. **87**, pp. 136–145, 2015.

Garoosi, F., Bagheri, G., and Rashidi, M.M., Two phase simulation of natural convection and mixed convection of the nanofluid in a square cavity, *Powder Technol.*, vol. **275**, pp. 239–256, 2015.

Hamad, M.A.A., Uddin, Md.J., and Ismail, M.I.Md., Radiation effects on heat and mass transfer in MHD stagnation-point flow over a permeable flat plate with thermal convective surface boundary condition, temperature dependent viscosity and thermal conductivity, *Nuclear Eng. Des.*, vol. **242**, pp. 194–200, 2012.

Harris, S.D., Ingham, B.D., and Pop, I., Mixed convection boundary-layer flow near the stagnation point on a vertical surface in a porous medium: Brinkman model with slip, *Transp. Porous Media*, vol. **77**, pp. 267–285, 2009.

Hayat, T., Shehzad, S.A., Alsaedi, A., and Alhothuali, M.S., Mixed convection stagnation point flow of Casson fluid with convective boundary conditions, *Chin. Phys. Lett.*, vol. **29**, 114704, 2012.

Hong, J.T., Yamada, Y., and Tien, C.L., Effects of non-Darcian and non-uniform porosity on vertical plate natural convection in porous media, *ASME J. Heat Transfer*, vol. **109**, pp. 356–362, 1987.

Isa, S.P.M., Arifin, N.M., and Nazar, R., Mixed convection boundary layer flow of a Casson fluid near the stagnation point over a permeable surface, *Malay. J. Fund. Appl. Sci.*, vol. **10**, pp. 22–27, 2014.

Ishak, A., Nazar, R., and Pop, I., Dual solutions in mixed convection flow near a stagnation point on a vertical surface in a porous medium, *Int. J. Heat Mass Transfer*, vol. **51**, pp. 1150–1155, 2008.

Khan, M., Hashim, Hussain, M., and Azam, M., Magnetohydrodynamic flow of carreau fluid over a convectively heated surface

in the presence of non-linear radiation, *J. Magn. Magn. Mater.*, vol. **412**, pp. 63–68, 2016.

Khan, W.A. and Pop, I., Boundary-layer flow of a nanofluid past a stretching sheet, *Int. J. Heat Mass Transfer*, vol. **53**, pp. 2477–2483, 2010.

Liu, Z., Liu, Y., Chang, Y., Seyf, H.R., Henry, A., Mattheyses, A.L., Yehl, K., Zhang, Y., Huang, Z., and Salaita, K., Nanoscale optomechanical actuators for controlling mechanotransduction in living cells, *Nature Methods*, vol. **13**, pp. 143–146, 2016.

Maleque, Kh.A., Effects of binary chemical reaction and activation energy on MHD boundary layer heat and mass transfer flow with viscous dissipation and heat generation/absorption, *ISRN Thermodyn*., vol. **2013**, pp. 1–9, 2013a.

Maleque, Kh.A., Effects of exothermic/endothermic chemical reactions with arrhenius activation energy on MHD free convection and mass transfer flow in presence of thermal radiation, *J. Thermodyn.*, vol. **2013**, pp. 1–11, 2013b.

McDonald, D.A., *Blood Flows in Arteries*, 2nd edition, Chap. 2, London: Arnold, 1974.

Mustafa, M., Hayat, T., Pop, I., and Hendi, A.A., Stagnation-point flow and heat transfer of a Casson fluid towards a stretching sheet, *Z. Naturforsch.*, vol. **67**, pp. 70–76, 2012.

Nield, D.A. and Kuznetsov, A.V., The Cheng–Minkowycz problem for natural convective boundary-layer flow in a porous medium saturated by a nanofluid, *Int. J. Heat Mass Transfer*, vol. **52**, pp. 5792–5795, 2009.

Nield, D.A. and Kuznetsov, A.V., Natural convective boundary-layer flow of a nanofluid past a vertical plate, *Int. J. Therm. Sci.*, vol. **49**, pp. 243–247, 2010.

Pantokratoras, A., Mixed convection in a Darcy–Brinkman porous medium with a constant convective thermal boundary condition, *Transp. Porous Media*, vol. **104**, pp. 273–288, 2014.

Pantokratoras, A., Forced convection in a Darcy–Brinkman porous medium with a convective thermal boundary condition, *J. Porous Med*., vol. **18**, no. 9, pp. 873–878, 2015.

Prasad, K.V., Vajravelu, K., and Vaidya, H., MHD Casson nanofluid flow and heat transfer at a stretching sheet with variable thickness, *J. Nanofluids*, vol. **5**, pp. 423–435, 2016a.

Prasad, K.V., Vajravelu, K., Shivakumara, I.S., Vaidya, H., and Basha, N.Z., Flow and heat transfer of a Casson nanofluid over a nonlinear stretching sheet, *J. Nanofluids*, vol. **5**, pp. 743–752, 2016b.

Prasad, K.V., Vajravelu, K., Vaidya, H., Basha, N.Z., and Umesh, V., Thermal and species concentration of MHD Casson fluid at a vertical sheet in the presence of variable fluid properties, *Ain Shams Eng. J.*, 2017. DOI: 10.1016/j.asej.2016.08.017

Rana, P. and Bhargava, R., Flow and heat transfer of a nanofluid over a nonlinearly stretching sheet: A numerical study, *Commun. Nonlin. Sci. Numer. Simul.*, vol. **17**, pp. 212–226, 2012.

Rashidi, M.M., Abelman, S., and Freidoonimehr, N., Entropy generation in steady MHD flow due to a rotating porous disk in a nanofluid, *Int. J. Heat Mass Transfer*, vol. **62**, pp. 515–525, 2013.

Rashidi, M.M., Hosseini, A., Pop, I., Kumar, S., and Freidoonimehr, N., Comparative numerical study of single and two-phase models of nanofluid heat transfer in wavy channel, *Appl. Math. Mech*., vol. **35**, pp. 831–848, 2014.

Rassoulinejad-Mousavi, S.M. and Abbasbandy, S., Analysis of forced convection in a circular tube filled with a Darcy-Brinkman-Forchheimer porous medium using spectral homotopy analysis method, *ASME J. Fluids Eng*., vol. **133**, 101207, 2011.

Rassoulinejad-Mousavi, S.M., Abbasbandy, S., and Alsulami, H.H., Analytical flow study of a conducting maxwell fluid through a porous saturated channel at various wall boundary conditions, *Eur. Phys. J. Plus*, vol. **129**, pp. 1–10, 2014.

Rassoulinejad-Mousavi, S.M., Mao, Y., and Zhang, Y., Evaluation of copper, aluminum, and nickel interatomic potentials on predicting the elastic properties, *AIP J. Appl. Phys*., vol. **119**, 244304, 2016.

Rassoulinejad-Mousavi, S.M.R., Seyf, H.R., and Abbasbandy, S., Heat transfer through a porous saturated channel with permeable walls using two-equation energy model, *J. Porous Media*, vol. **16**, pp. 241–254, 2013.

Rassoulinejad-Mousavi, S.M. and Yaghoobi, H., Effect of non-linear drag term on viscous dissipation in a fluid saturated porous medium channel with various boundary conditions at walls, *Arabian J. Sci. Eng*., vol. **39**, pp. 1231–1240, 2014.

Rahman, S.-ur, Haq, R.-ul, Khan, Z.H., and Lee, C., Entropy generation analysis for non-Newtonian nanofluid with zero normal flux of nanoparticles at the stretching surface, *J. Taiwan Inst. Chem. Eng*., vol. **63**, pp. 226–236, 2016.

Rosali, H., Ishak, A., and Pop, I., Mixed convection stagnation-point flow over a vertical plate with prescribed heat flux embedded in a porous medium: Brinkman-extended Darcy formulation, *Transp. Porous Media*, vol. **90**, pp. 709–719, 2011.

Seyf, H.R. and Rassoulinejad-Mousavi, S.M., An analytical study for fluid flow in porous media imbedded inside a channel with moving or stationary walls subjected to injection/suction, *ASME J. Fluids Eng*., vol. **133**, 091203, 2011.

Shafique, Z., Mustafa, M., and Mushtaq, A., Boundary layer flow of Maxwell fluid in rotating frame with binary chemical reaction and activation energy, *Results Phys*., vol. **6**, pp. 627–633, 2016.

Shaw, S., Gorla, R.S.R., Murthy, P.V.S.N., and Ng, C.O., Pulsatile Casson fluid flow through a stenosed bifurcated artery, *Int. J. Fluid Mech. Res.*, vol. **36**, pp. 43–63, 2009.

Shehzad, S.A., Hayat, T., Qasim, M., and Asghar, S., Effects of mass transfer on MHD flow of Casson fluid with chemical reaction and suction, *Braz. J. Chem. Eng.*, vol. **30**, pp. 187–195, 2013.

Shirazpour, A., Rassoulinejad-Mousavi, S.M., and Seyf, H.R., HPM solution of momentum equation for Darcy-Brinkman model in a parallel plates channel subjected to Lorentz force, *Int. Conf. Fluid Mech. Heat Transfer Thermodyn*., vol. **5**, pp. 258–262, 2011.

Vadasz, P., *Emerging Topics in Heat and Mass Transfer in Porous Media*, New York: Springer, 2008.

Vafai, K., *Handbook of Porous Media*, 2nd edition, New York: Taylor & Francis, 2005.

Vajravelu, K., Prasad, K.V., Ng, C.O., and Umesh, V., MHD squeeze flow and heat transfer of a nanofluid between parallel discs with variable fluid properties and transpiration, *Int. J. Mech. Mater. Eng*., vol. **12**, p. 9, 2017.

Yacob, N.A., Ishak, A., and Pop, I., Falkner-skan problem for a static or moving wedge in nanofluids, *Int. J. Therm. Sci*., vol. **50**, pp. 133–139, 2011.

Zaib, A., Bhattacharyya, K., Uddin, Md.S., and Shafie, S., Dual solutions of non-Newtonian Casson fluid flow and heat transfer over an exponentially permeable shrinking sheet with viscous dissipation, *Model. Simul. Eng.*, vol. **2016**, pp. 1–8, 2016.